# Interference between two independent multi-temporal-mode thermal fields

Jie Su,[1] Jiamin Li,[1] Liang Cui,[1] Xiaoying Li,[1,*] and Z. Y. Ou[1,2,†]

[1]*School of Precision Instrument and Opto-electronics Engineering, Tianjin University, Key Laboratory of Opto-Electronic Information*
*Technology of Ministry of Education, Tianjin 300072, China*
[2]*Department of Physics, Indiana University-Purdue University Indianapolis, 402 N. Blackford St., Indianapolis, Indiana 46202, USA*

We construct a general theoretical model for analyzing the intensity correlation of the field formed by mixing two independent multi-temporal-mode thermal fields. In the model, we use the intensity correlation function $g^{(2)}$ to characterize the mode property of the mixed thermal field. We find that $g^{(2)}$ of the mixed field is always less than that of the individual thermal field with less average mode number unless the two thermal fields are identical in mode property. The amount of drop in $g^{(2)}$ of the interference field depends on the relative overlap between the mode structures of two thermal fields and their relative strength. We successfully derive the analytical expressions of the upper bound and lower limit for $g^{(2)}$ of the interference field. Moreover, we verify the theoretical analysis by performing a series of experiments when the mode structures of two independent thermal fields are identical, orthogonal, and partially overlapped, respectively. The experimental results agree with theoretical predictions. Our investigation is useful for analyzing the signals carried by the intensity correlation of thermal fields.

## I. INTRODUCTION

In nature, most light sources are of thermal feature because of the randomness of individual emitters [1]. Therefore, what we see often is mostly the addition of many thermal sources. When two independent thermal fields are mixed or combined, one usually thinks that there is no interference between them and the result is simply the addition of the two. This is true at intensity level. However, this is not true at higher-order measurement such as intensity correlation.

Photon bunching effect, observed by Hanbury Brown and Twiss (HBT) in 1956 [2], is the first observed higher-order effect in the form of intensity correlation due to the intensity fluctuations of a thermal optical field. The HBT effect is the basis for the technique of ghost imaging [3–5], where higher-order quantities such as intensity correlations of thermal sources are measured and the excess intensity correlation beyond random intensity correlation serves as the signal for characterizing an image.

When two independent optical fields are mixed, even though intensity shows no interference, the measurement of high-order quantities such as intensity correlations does produce an interference pattern [6], which is known as "fourth-order interference" or later called "two-photon interference" [7]. So, when the signal is carried by an optical field and extracted out by intensity measurement, the background noise which usually possesses the thermal nature can be simply subtracted out. But if the optical signals need to be extracted from intensity correlation measurement, such as those in the ghost image techniques for thermal fields, the problem of mixing two independent thermal sources becomes prominent:

if both the background noise and the signal fields are in thermal states, the effect of fourth-order interference between signal and background fields will show up. In this case, the fourth-order interference effect is reflected by the excess intensity correlation and the background noise cannot be easily taken out. Furthermore, since the signal is extracted from the excess correlations of thermal sources, the excess correlation as large as possible is desired to achieve a good signal-to-noise ratio (SNR) measurement. But the fourth-order interference between the signal field and background noise will definitely affect the excess intensity correlation and therefore the SNR extracted in ghost imaging technique.

It has been shown that the visibility of fourth-order interference between two independent thermal sources $V$ is closely related to the intensity correlation function $g^{(2)}$ of each thermal source, and the maximum value of $V$ is 1/3 [8–10]. The maximum visibility 1/3 can be obtained either by using detectors with response time much faster than the coherence time of thermal fields or by using thermal fields in single mode. Since the response time of detectors used to measure $g^{(2)}$ is usually much longer than the coherence time of detected optical field, $g^{(2)}$ can also be viewed as a quantity for characterizing the mode number of thermal field [1,9,10]. So far, most investigations on the interference between thermal sources are based on single-mode models under the ideal conditions which give rise to the maximum photon bunching effect of $g^{(2)} = 2$. However, the multi-mode nature of the thermal sources will reduce the photon bunching effect, i.e., $g^{(2)}$ decreases with the increase of mode number of thermal source. So the interference effect between two thermal sources or the photon bunching effect of the interference field will be certainly affected by the mode property.

On the other hand, the mode properties of optical fields are sometimes complicated and cannot be characterized easily. This is because the two fields participating in interference

---------
*xiaoyingli@tju.edu.cn
†zheyuou@tju.edu.cn

such as the signal field and the background noise may have different mode structures and mode numbers. So far, quantitative research on the higher-order interference between two multi-mode thermal fields has not been fulfilled yet. In this paper, we will study how the temporal mode structures and relative intensity of two independent thermal fields affect the intensity correlation function of the interference field. Moreover, we perform experiments to verify our theoretical prediction.

The rest of the paper is organized as follows. In Sec. II, we theoretically study the influence of mode structure of two thermal fields, which are in single spatial mode and multi-temporal mode, upon the two-photon interference effect shown in their interference field. We derive the formulas, which describe the upper bound and lower limit of $g^{(2)}$, for the interference field formed by combining two multi-temporal-mode thermal fields. In Sec. III, we demonstrate the experimental verification, in which the interference effect of two multi-temporal-mode thermal fields with identical mode structure and different mode structures are measured and analyzed. Conclusions and discussion are presented in the last section.

## II. GENERAL THEORETICAL ANALYSIS

The mode number of a multi-mode thermal field, reflected by its photon statistics, can be characterized by normalized intensity correlation function. Beginning with a brief review of the photon statistics for a thermal field, which is in single spatial mode and multi-temporal mode, we will study the mode property of the interference field formed by mixing two independent thermal sources. The results indicate that the mode property of interference field depends on the two-photon interference between two thermal sources. Moreover, we will analyze the factors influencing the two-photon interference.

### A. Photon statistics for a thermal field in multi-temporal modes

A thermal light field is a random process with complex Gaussian probability distribution [1]. Its description, however, depends on the mode structure employed. For the stationary field of continuous wave, a common approach of distinguishing the modes is by frequency [11]. For nonstationary fields of pulses, it is better to work in the time domain with orthogonal broadband wave-packet modes, known as "temporal modes" (TMs) [12], especially for the ultrashort pulses with pulse durations much shorter than the response time of detectors. Indeed, for the fields confined by the waveguide with single-transverse mode, such as standard single mode optical fiber, the TMs form a complete basis for representing an arbitrary pulsed multi-mode optical field.

The photon statistic of a thermal field can be characterized by the Hanbury Brown–Twiss interferometer [9,13], consisting of a 50:50 beam splitter (BS) and two detectors (D1 and D2), as shown in Fig. 1(a). For a nonstationary field $\vec{E}(t)$ with a quasi-continuous wave (quasi-cw) train of pulses, the field has the form of

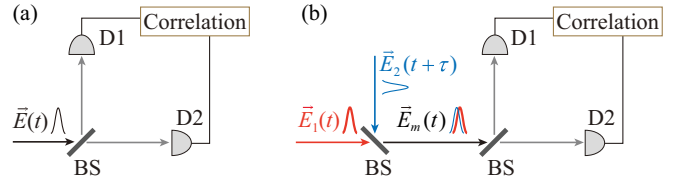$$\vec{E}(t) = \vec{e} \sum_i E_i(t - i\Delta T), \quad (1)$$



FIG. 1. Schematic of Hanbury Brown–Twiss (HBT) interferometer for intensity correlation measurements of (a) a thermal field and (b) an interference field formed by mixing two individual thermal fields, respectively. BS, 50:50 beam splitter; D, detector.

where $\vec{e}$ is the unit polarization vector, $E_i(t)$ is the $i$th single pulse profile with a pulse width $\delta t$, and $\Delta T (\gg \delta t)$ is the interval between two adjacent pulses. Then the instantaneous intensity is

$$I(t) = |\vec{E}(t)|^2 = \sum_{i,j} E_i^*(t - i\Delta T)E_j(t - j\Delta T)$$

$$= \sum_i |E_i(t - i\Delta T)|^2. \quad (2)$$

We assume the detectors have the same response function $k(t)$ $[k(t) = 0$ for $t < 0]$, which has a response time $T_r$ much smaller than the pulse interval $(T_r \ll \Delta T)$ but much larger than the pulse width $(T_r \gg \delta t)$. Then the photocurrents from the two detectors (D1 and D2) are [14]

$$i_{D1}(t) = i_{D2}(t) = \int_{-\infty}^{\infty} d\tau \, k(\tau - t)I(\tau)/2$$

$$= \frac{1}{2} \sum_i k(t - i\Delta T)I_i, \quad (3)$$

with the factor of $1/2$ from the BS and

$$I_i \equiv \int_{-\infty}^{\infty} dt |E_i(t)|^2 \quad (4)$$

is the integrated intensity of the $i$th pulse. Under this condition, the average current measured by D1 and D2 for a period $T$ covering many pulses can be written as

$$\langle i_{D1} \rangle_T = \langle i_{D2} \rangle_T = \frac{1}{T} \int_T i_{D1,D2}(t)dt = \frac{1}{2} R_p Q \langle I_i \rangle_e, \quad (5)$$

where $Q \equiv \int k(t)dt$ is the total charge for one pulse and $R_p = 1/\Delta T$ is the repetition rate of the pulses. The subscripted angle bracket $\langle \cdot \rangle_e$ is the ensemble average over $i$ from pulse to pulse over the time interval $T$: $\langle I_i \rangle_e = (1/N) \sum_i I_i$ with $N = [T/\Delta T]$ as the number of pulses in time interval $T$. So, the average photocurrent is independent of time and $\langle i_{D1} \rangle_T = \langle i_{D2} \rangle_T \propto \langle I_i \rangle_e / 2$, where $\langle I_i \rangle_e / 2$ is the average intensity at D1, D2. For intensity correlation between the two detectors D1 and D2, however, the outcome depends on the delay $\Delta t$ between the detectors:

$$\langle i_{D1}(t)i_{D2}(t + \Delta t) \rangle_T = \frac{1}{T} \int_T i_{D1}(t)i_{D2}(t + \Delta t)dt$$

$$= \frac{1}{4} R_p K(\Delta t) \langle I_i I_{i+n} \rangle_e, \quad (6)$$

where $K(\Delta t) \equiv \int dt\, k(t)k(t + \Delta t - n\Delta T)$ and $n = [\Delta t / \Delta T]$ is the number of pulses during the delay $\Delta t$. So, the intensity correlation measurement gives a spiked delay dependent function $K(\Delta t)$, which is spaced by the pulse interval $\Delta T$ but has two different peak values. When $\Delta t = 0$, the first peak value is the autocorrelation describing pulse intensity fluctuation:

$$\Gamma^{(2)}(0) \equiv \langle i_{D1}(t) i_{D2}(t) \rangle_T = \frac{1}{4} R_p K(0) \langle I_i^2 \rangle_e, \qquad (7)$$

but when $\Delta t = n\Delta T$ $(n = 1, 2, 3, \ldots)$, the spike at the nonzero delay has a different peak value which is the cross-pulse correlation describing intensity fluctuation between different pulses:

$$\Gamma^{(2)}(\Delta T) \equiv \langle i_{D1}(t) i_{D2}(t + n\Delta T) \rangle_T = \frac{1}{4} R_p K(0) \langle I_i I_{i+n} \rangle_e. \qquad (8)$$

Since the pulses are independent of each other, their fluctuations are uncorrelated so that $\langle I_i I_{i+n} \rangle_e = \langle I_i \rangle_e \langle I_{i+n} \rangle_e = \langle I_i \rangle_e^2$. We then obtain the normalized intensity correlation function for quasi-cw pulsed fields in HBT measurement [15,16]:

$$g^{(2)}(0) = g^{(2)} \equiv \frac{\Gamma^{(2)}(0)}{\Gamma^{(2)}(\infty)} = \frac{\Gamma^{(2)}(0)}{\Gamma^{(2)}(\Delta T)} = \frac{\langle I_i^2 \rangle_e}{\langle I_i \rangle_e^2}$$

$$= \frac{\int_{-\infty}^{\infty} dt \int_{-\infty}^{\infty} dt' \langle E_i^*(t) E_i^*(t') E_i(t') E_i(t) \rangle_e}{\int_{-\infty}^{\infty} dt \langle E_i^*(t) E_i(t) \rangle_e \int_{-\infty}^{\infty} dt' \langle E_i^*(t') E_i(t') \rangle_e}. \qquad (9)$$

As we will see later, the value of $g^{(2)}(0)$ is determined by the mode property of the pulsed field $\vec{E}(t)$ [9,10]. For the sake of brevity, we omit the lower and upper limits of the time integrals and use $g^{(2)}$ to represent $g^{(2)}(0)$ and $E(t)$ for $E_i(t)$ hereinafter.

It is well known that, for a thermal optical field propagating in single-mode waveguide, one-dimensional approximation applies. Under this condition, the vector electric-field amplitude in the temporal mode basis can be written as

$$\vec{E}(t) = \vec{e} \sum_i A_i \phi_i(t), \qquad (10)$$

where $\phi_i(t) = \frac{1}{\sqrt{2\pi}} \int_{-\infty}^{\infty} f_i(\omega) e^{-i\omega t} d\omega$ is the temporal mode profile for mode $i$ with continuous spectrum $f_i(\omega)$ and $A_i$ denotes the complex amplitude of temporal mode $i$, which is a random variable with Gaussian distribution. In Eq. (10), because of the phase randomness of thermal radiations, we have $\langle A_i \rangle_e = 0$ and $\langle A_i^* A_j \rangle_e = 0$ $(i \neq j)$ for $i, j = 1, 2, \ldots$. The intensity distributed in mode $\phi_i(t)$ is described by $\langle |A_i|^2 \rangle_e = \alpha_i^2$. For higher-order average, assuming different modes are independent, we have

$$\langle |A_i|^2 |A_j|^2 \rangle_e = \langle |A_i|^2 \rangle_e \langle |A_j|^2 \rangle_e = \alpha_i^2 \alpha_j^2 \quad \text{for } i \neq j. \qquad (11)$$

Because of the Gaussian distribution, we can use Isserlis' theorem [17] for the higher-order moment:

$$\langle |A_i|^4 \rangle_e = \langle A_i^* A_i^* A_i A_i \rangle_e$$
$$= \langle A_i^* A_i^* \rangle_e \langle A_i A_i \rangle_e + \langle A_i^* A_i \rangle_e \langle A_i^* A_i \rangle_e$$
$$+ \langle A_i^* A_i \rangle_e \langle A_i A_i^* \rangle_e$$
$$= 2\alpha_i^4. \qquad (12)$$

Although the TMs can be fully overlapped in polarization, space, frequency, and time, TMs are orthogonal to each other
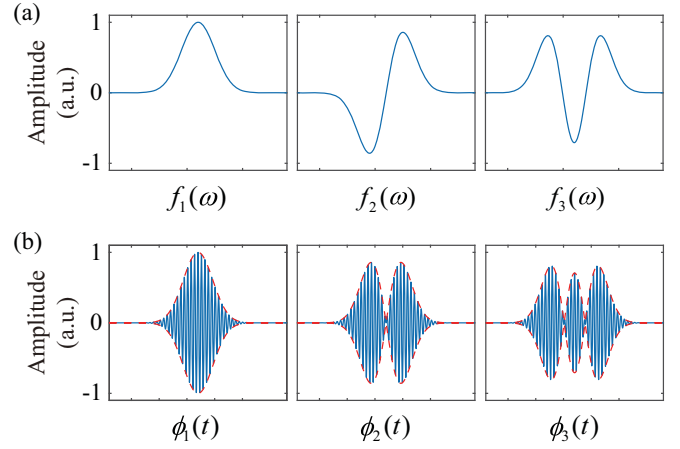


FIG. 2. First three Hermite-Gaussian modes of a temporal mode basis in (a) frequency domain and (b) time domain, respectively.

with respect to a time (frequency) integral:

$$\int_{-\infty}^{\infty} dt\, \phi_i^*(t) \phi_j(t) = \frac{1}{2\pi} \int_{-\infty}^{\infty} d\omega\, f_i^*(\omega) f_j(\omega) = \delta_{i,j}. \qquad (13)$$

In order to show how the temporal modes (TMs) look, we exemplarily plot the first three members of a TM basis in which $f_i(\omega)$ represents a family of Hermite-Gaussian functions, as shown in Fig. 2.

To investigate the temporal mode property of thermal field $\vec{E}(t)$ described by Eq. (10), we substitute Eq. (10) into Eq. (9) and use the relationship of Eq. (13) which results in the time integral to become a $\delta$ function. As a result, the average intensity per pulse is

$$\langle I \rangle_e = \int dt \langle \vec{E}^*(t) \cdot \vec{E}(t) \rangle_e = \sum_i \langle |A_i|^2 \rangle_e = \sum_i \alpha_i^2, \qquad (14)$$

and the higher-order average is

$$\langle I^2 \rangle_e = \int dt\, dt' \langle \vec{E}^*(t) \cdot \vec{E}(t) \vec{E}^*(t') \cdot \vec{E}(t') \rangle_e$$
$$= \sum_{i,j} \langle |A_i|^2 |A_j|^2 \rangle_e$$
$$= \sum_i \langle |A_i|^4 \rangle_e + \sum_{i \neq j} \langle |A_i|^2 |A_j|^2 \rangle_e. \qquad (15)$$

Substituting Eqs. (14) and (15) into Eq. (9) and using Eqs. (11) and (12), we obtain the intensity correlation function for an individual multi-temporal-mode thermal field:

$$g^{(2)} = \frac{\left[ \sum_i \alpha_i^4 + \left( \sum_i \alpha_i^2 \right)^2 \right]}{\left( \sum_i \alpha_i^2 \right)^2}$$
$$= 1 + \frac{\sum_i \alpha_i^4}{\left( \sum_i \alpha_i^2 \right)^2} = 1 + \frac{1}{M}, \qquad (16)$$

where $M \equiv (\sum_i \alpha_i^2)^2 / \sum_i \alpha_i^4$ is the average temporal mode number of thermal field $\vec{E}(t)$. Equation (16) shows the intensity correlation function $g^{(2)}$ is determined by the average

temporal mode number $M$. For a single-mode field, we have $M = 1$ and $g^{(2)}$ has the maximum value of 2. In this case, the photon bunching effect of the thermal field is maximized. Moreover, if we assume the intensity of the field is equally distributed in each mode, i.e., $\alpha_i^2 = \alpha^2 = I_0$ for $i = 1, \ldots, M$ with $M$ denoting the number of mode, the average intensity measured by D1 (D2) can be calculated from Eqs. (4), (5), and (14) as $\langle I_{D1}(t) \rangle = \langle I_{D2}(t) \rangle = \frac{1}{2} \langle I \rangle_e = \frac{1}{2} M I_0$.

## B. Photon statistics for a field formed by mixing two multi-temporal-mode thermal fields

Now we study the property of a field formed by mixing two independent multi-temporal-mode thermal fields. As shown in Fig. 1(b), the mixed field $\vec{E}_m(t)$ obtained by mixing two fields $\vec{E}_1$ and $\vec{E}_2$ with a 50:50 BS is written as

$$
\begin{aligned}
\vec{E}_m(t) &= [\vec{E}_1(t) + \vec{E}_2(t+\tau)]/\sqrt{2} \\
&= [\vec{e}_1 E_1(t) + \vec{e}_2 E_2(t+\tau)]/\sqrt{2},
\end{aligned} \tag{17}
$$

with

$$
E_1(t) = \sum_i A_i \phi_i(t), \tag{18}
$$

$$
E_2(t+\tau) = \sum_k B_k \varphi_k(t+\tau), \tag{19}
$$

where $\varphi_k(t) = \frac{1}{\sqrt{2\pi}} \int_{-\infty}^{\infty} g_k(\omega) e^{-i\omega t} d\omega$ is the temporal mode profile for mode $k$ with continuous spectrum $g_k(\omega)$ for $E_2$ field, $\vec{e}_{1,2}$ is the unit polarization vector, and $\tau$ denotes the relative delay between the two fields when they combined at BS. Because $A_i$ and $B_k$ are independent complex Gaussian random variables, the following relations hold:

$$
\langle A_i \rangle_e = \langle B_k \rangle_e = 0, \quad \langle A_i^* B_k \rangle_e = \langle B_i^* A_k \rangle_e = 0,
$$

$$
\langle A_i^* A_j \rangle_e = \delta_{i,j} \alpha_i^2, \quad \langle B_k^* B_l \rangle_e = \delta_{k,l} \beta_k^2,
$$

$$
\langle |A_i|^2 |B_j|^2 \rangle_e = \alpha_i^2 \beta_j^2, \quad \langle |A_i|^2 |A_j|^2 \rangle_e = (1 + \delta_{i,j}) \alpha_i^2 \alpha_j^2,
$$

$$
\langle |B_k|^2 |B_l|^2 \rangle_e = (1 + \delta_{k,l}) \beta_k^2 \beta_l^2. \tag{20}
$$

The overlap for the TMs structure of $E_1$ and $E_2$ is described by the integral of their mode bases:

$$
K_{ik} \equiv \int_{-\infty}^{\infty} dt \, \phi_i^*(t) \varphi_k(t+\tau) \leqslant 1. \tag{21}
$$

When the mode bases of $E_1$ and $E_2$ are perfectly overlapped, i.e., $\phi_k(t) = \varphi_k(t+\tau)$, we have $K_{ik} = \delta_{i,k}$.

The photon statistics of the mixed field $\vec{E}_m(t)$ is characterized by using an HBT interferometer, as shown in Fig. 1(b). The instantaneous intensity of the mixed field is

$$
\begin{aligned}
\vec{E}_m^*(t) \cdot \vec{E}_m(t) = [&|E_1(t)|^2 + |E_2(t+\tau)|^2 \\
&+ \cos\theta \, E_1^*(t) E_2(t+\tau) \\
&+ \cos\theta \, E_2^*(t+\tau) E_1(t)]/2,
\end{aligned} \tag{22}
$$

where $\cos\theta = \vec{e}_1 \cdot \vec{e}_2$ describes the overlap of the polarization modes between $E_1$ and $E_2$. By substituting Eq. (22) into Eq. (4) and performing time integral and the ensemble average, we arrive at the average intensity measured by D1

and D2

$$
\begin{aligned}
\frac{1}{2} \langle I_m \rangle_e &= \frac{1}{2} \int dt \langle \vec{E}_m^*(t) \cdot \vec{E}_m(t) \rangle_e \\
&= \frac{1}{4} \left[ \sum_i \langle |A_i|^2 \rangle_e + \sum_k \langle |B_k|^2 \rangle_e \right] \\
&= \frac{1}{4} \left( \sum_i \alpha_i^2 + \sum_k \beta_k^2 \right).
\end{aligned} \tag{23}
$$

Equation (23) clearly shows that the intensity is simply the addition of two fields and no interference effect has shown up. However, the intensity correlation function between the two detectors becomes

$$
\begin{aligned}
\frac{1}{4} \langle I_m^2 \rangle_e &= \frac{1}{4} \int dt \, dt' \langle \vec{E}_m^*(t) \cdot \vec{E}_m(t) \vec{E}_m^*(t') \cdot \vec{E}_m(t') \rangle_e \\
&= \frac{1}{16} \left( \sum_i \alpha_i^2 + \sum_k \beta_k^2 \right)^2 + \frac{1}{16} \left( \sum_i \alpha_i^4 + \sum_k \beta_k^4 \right. \\
&\quad \left. + 2 \cos^2\theta \sum_{i,k} \alpha_i^2 \beta_k^2 |K_{ik}|^2 \right),
\end{aligned} \tag{24}
$$

where $\cos^2\theta \sum_{i,k} \alpha_i^2 \beta_k^2 |K_{ik}|^2$ is the interference term. Accordingly, we obtain the normalized intensity correlation function of the mixed thermal field:

$$
\begin{aligned}
g_m^{(2)} &= 1 + \frac{\sum_i \alpha_i^4 + \sum_k \beta_k^4 + 2 \cos^2\theta \sum_{i,k} \alpha_i^2 \beta_k^2 |K_{ik}|^2}{\left( \sum_i \alpha_i^2 + \sum_k \beta_k^2 \right)^2} \\
&= 1 + \frac{1}{M_m},
\end{aligned} \tag{25}
$$

where

$$
M_m = \frac{(\bar{I}_1 + \bar{I}_2)^2}{\sum_i \alpha_i^4 + \sum_k \beta_k^4 + 2 \cos^2\theta \sum_{i,k} \alpha_i^2 \beta_k^2 |K_{ik}|^2} \tag{26}
$$

denotes the average mode number of the mixed interference field. From Eq. (26), one sees that, although the intensities of the individual fields, $\bar{I}_1 = \sum_i \alpha_i^2$ and $\bar{I}_2 = \sum_k \beta_k^2$, are influencing factors, the key determining $M_m$ is the interference term $\cos^2\theta \sum_{i,k} \alpha_i^2 \beta_k^2 |K_{ik}|^2$, in which the coefficients $\theta$ and $K_{ik}$, respectively describing the overlap of polarization and mode structures of TMs between $E_1$ and $E_2$, play an important role. To better understand the factors affecting mode property of the interference field, we analyze the dependence of $g_m^{(2)}$ in Eq. (25) in the following three cases.

In the first case, the mode structures and polarization of the two independent fields $E_1$ and $E_2$ are identical, the interference term $\cos^2\theta \sum_{i,k} \alpha_i^2 \beta_k^2 |K_{ik}|^2$ in Eqs. (25) and (26) takes the maximum value, i.e., $\cos\theta = 1$ and $K_{ik} = \delta_{i,k}$. Under such conditions, Eq. (25) has the simplified form

$$
g_m^{(2)} = 1 + \frac{\sum_i \left( \alpha_i^2 + \beta_i^2 \right)^2}{\left[ \sum_i \left( \alpha_i^2 + \beta_i^2 \right) \right]^2}. \tag{27}
$$

It is obvious that, for $\beta_i = 0$ or $\alpha_i = 0$, the mixed interference field becomes the individual field $E_1$ or $E_2$. Under this situation, $g_m^{(2)} = g_1^{(2)} = 1 + \frac{1}{M_1}$ or $g_m^{(2)} = g_2^{(2)} = 1 + \frac{1}{M_2}$, which are consistent with the photon statistics for a thermal field

[see Eq. (16)]. Here $M_1$ and $M_2$ refer to the mode numbers of fields $E_1$ and $E_2$, respectively. Since it is difficult to obtain an analytical solution from the general expression in Eq. (27), we assume $M_1 \leqslant M_2$ and the intensities for both $E_1$ and $E_2$ are equally distributed in each TM, i.e.,

$$\alpha_i = \alpha \ (i = 1, \ldots, M_1), \quad \beta_k = \beta \ (k = 1, \ldots, M_2). \quad (28)$$

Under the assumptions in Eq. (28), Eq. (27) can be approximated as

$$\begin{aligned} g_m^{(2)} &= 1 + \frac{M_1(\alpha^2 + \beta^2)^2 + (M_2 - M_1)\beta^4}{(M_1\alpha^2 + M_2\beta^2)^2} \\ &= 1 + \frac{\mathcal{R}^2}{M_1} + \frac{1 - \mathcal{R}^2}{M_2}, \end{aligned} \quad (29)$$

with the relative intensity coefficient

$$\mathcal{R} = \frac{\bar{I}_1}{\bar{I}_1 + \bar{I}_2}, \quad (30)$$

where $\bar{I}_1 = M_1\alpha^2$ and $\bar{I}_2 = M_2\beta^2$ are the intensity of two independent thermal fields. Equation (29) can be viewed as the upper bound for the two-photon interference showing up in the interference field. When $M_1 = M_2$, the mode of the interference filed is the same as that of the individual field and is irrelevant to $\mathcal{R}$, i.e., $g_m^{(2)} = g_1^{(2)} = g_2^{(2)}$ always holds. When $M_1 < M_2$, however, $g_m^{(2)}$ decreases from $g_1^{(2)}$ to $g_2^{(2)}$ with the decrease of $\mathcal{R}$ and reaches the minimum $g_m^{(2)} = g_2^{(2)}$ at $\mathcal{R} = 0$.

In the second case, the modes of two independent fields $E_1$ and $E_2$ are orthogonal; the interference term $\cos^2\theta \sum_{i,k} \alpha_i^2\beta_k^2|K_{ik}|^2$ in Eq. (25) takes the minimum value zero. This can be realized by two approaches: (i) the polarization of the two fields are perpendicular to each other ($\cos\theta = 0$) or (ii) there is no overlap between the TMs of $E_1$ and $E_2$ ($K_{ik} = 0$). Under such conditions, Eq. (25) is simplified as

$$g_m^{(2)} = 1 + \frac{\sum_i \alpha_i^4 + \sum_k \beta_k^4}{\left( \sum_i \alpha_i^2 + \sum_k \beta_k^2 \right)^2}. \quad (31)$$

Under the assumptions of $M_1 \leqslant M_2$ and Eq. (28), Eq. (31) can be approximated as

$$g_m^{(2)} = 1 + \frac{M_1\alpha^4 + M_2\beta^4}{(M_1\alpha^2 + M_2\beta^2)^2} = 1 + \frac{\mathcal{R}^2}{M_1} + \frac{(1-\mathcal{R})^2}{M_2}. \quad (32)$$

Equation (32) can be viewed as the lower limit for the two-photon interference shown in the interference field. The intensity correlation function of the interference field drops to the minimum $g_{\min}^{(2)} = 1 + \frac{1}{M_1 + M_2}$ when the relative intensity coefficient of the two fields takes the value of $\mathcal{R} = \frac{M_1}{M_1 + M_2}$. In particular, for $M_1 = M_2 = M$, we have the minimum $g_m^{(2)}$ of $g_{\min}^{(2)} = 1 + \frac{1}{2M}$ for the two fields with equal intensity\rm ($\mathcal{R} = 0.5$).

In the third case, we have $\cos\theta = 1$ and $0 < K_{ik} < 1$. This is the most general situation for two independent thermal fields, because it is very easy to realize the perfect matching in polarization, however, it is impossible to perfectly match the TMs of two fields with $M_{1,2} > 1$ unless their emitting light

sources are identical. Under this condition, by defining

$$\mathcal{V} \equiv \frac{\sum_{i,k} \alpha_i^2\beta_k^2|K_{ik}|^2}{\sum_i \alpha_i^2\beta_i^2}, \quad (33)$$

Eq. (25) can be rewritten as

$$g_m^{(2)} = 1 + \frac{\sum_i \alpha_i^4 + \sum_k \beta_k^4 + 2\mathcal{V}\sum_i \alpha_i^2\beta_i^2}{\left( \sum_i \alpha_i^2 + \sum_k \beta_k^2 \right)^2}. \quad (34)$$

Moreover, by assuming $M_1 \leqslant M_2$ and taking the assumptions in Eq. (28), Eq. (34) can be approximated as

$$\begin{aligned} g_m^{(2)} &= 1 + \frac{M_1\alpha^4 + M_2\beta^4 + 2M_1\mathcal{V}\alpha^2\beta^2}{(M_1\alpha^2 + M_2\beta^2)^2} \\ &= 1 + \frac{\mathcal{R}^2}{M_1} + \frac{(1-\mathcal{R})(1 - \mathcal{R} + 2\mathcal{V}\mathcal{R})}{M_2}, \end{aligned} \quad (35)$$

where

$$\mathcal{V} = \frac{1}{M_1} \sum_{i=1,k=1}^{M_1,M_2} |K_{ik}|^2 \quad (36)$$

describes the mode overlap of two thermal fields. Because $\phi_i(t)$ and $\varphi_k(t)$ are complete bases of TMs for the thermal fields of $E_1$ and $E_2$, respectively, $K_{ik}$ in Eq. (36) is their transition matrix element which must satisfy $\sum_{k=all} |K_{ik}|^2 = 1$ so that

$$\sum_{k=1}^{M_2} |K_{ik}|^2 \leqslant \sum_{k=all} |K_{ik}|^2 = 1. \quad (37)$$

This leads to $\mathcal{V} \leqslant 1$. For the extreme cases discussed in the first case and second case, i.e., $K_{ik} = \delta_{i,k}$ and $K_{ik} = 0$ ($i = 1, \ldots, M_1; k = 1, \ldots, M_2$), the simplified form of Eq. (35) is exactly the upper bound and lower limit in Eqs. (29) and (32), respectively. In general, the TMs of $E_1$ and $E_2$ are partially overlapped; we have $0 < \mathcal{V} < 1$. From Eqs. (36) and (37), one sees that the value of $\mathcal{V}$ depends on $M_1$, $M_2$, and the details of the mode excitation through $K_{ik}$ quantities. Notice that Eqs. (35)–(37) are approximations under the assumption of Eq. (28), which is usually not the case for real thermal fields, so the experimental results presented in Sec. III B may only qualitatively agree with Eq. (35) when the general case of partial mode overlapping $0 < \mathcal{V} < 1$ is verified.

## III. EXPERIMENTAL VERIFICATION

We perform a few experiments to verify the theoretical results obtained in Sec. II. The experimental setup is shown in Fig. 3. The interference field $\vec{E}_m(t)$ is obtained by mixing two multi-mode thermal fields $\vec{E}_1(t)$ and $\vec{E}_2(t + \tau)$ with a 50:50 beam splitter (BS$_2$). The thermal fields $E_1$ and $E_2$ are respectively originated from two independent thermal sources (TSs). Each nonstationary TS is based on the radiation of $\chi^{(3)}$-based nonlinear process excited in dispersion shifted fiber (DSF) using a pulsed pump. The nonlinear process in DSF is either spontaneous Raman scattering (SRS) or spontaneous four wave mixing (SFWM). For the SRS, the imaginary part of $\chi^{(3)}$ couples the pump through thermally populated optical-phonon modes to Raman-scattering modes on the Stokes or anti-Stokes sides; for the SFWM, two
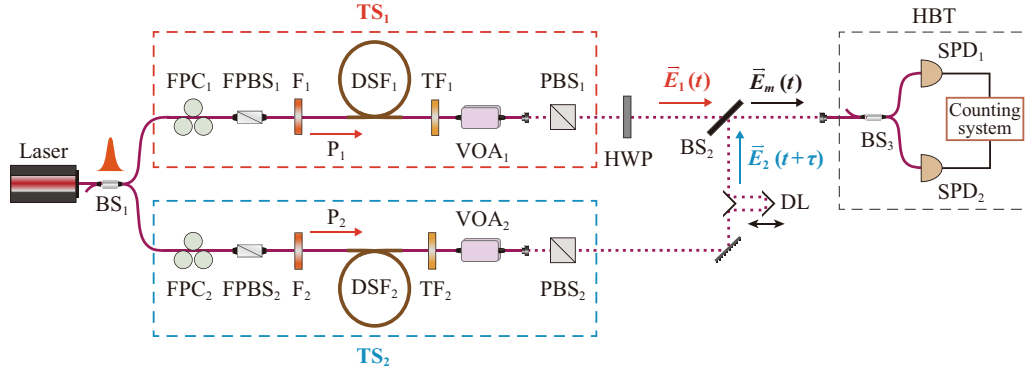
FIG. 3. Experimental setup for verifying the interference formed by mixing two multi-mode thermal fields $E_1$ and $E_2$. $P_1$-$P_2$, pump; $DSF_1$-$DSF_2$, dispersion shifted fiber; $F_1$-$F_2$, filter; $TF_1$-$TF_2$, tunable filter; $FPC_1$-$FPC_2$, fiber polarization controller; $FPBS_1$-$FPBS_2$, fiber polarization beam splitter; $PBS_1$-$PBS_2$, polarization beam splitter; $VOA_1$-$VOA_2$, variable optical attenuator; HWP, half wave plate; $BS_1$-$BS_3$, 50:50 beam splitter; DL, delay line; $SPD_1$-$SPD_2$, single photon detector. The solid lines and dotted lines in the scheme respectively denote the optical fiber propagation and free space propagation.

pump photons scatter through the real part of $\chi^{(3)}$ to create a simultaneous pair of Stokes and anti-Stokes photons. The Stokes waves originated from both SRS and SFWM are in thermal state [10,18]. In optical fibers, SRS with a broad gain bandwidth always occurs whenever the strong pump is propagating along optical fibers; however, the SFWM, which dominates over the SRS, occurs only when the phase matching condition of SFWM is satisfied [19].

For the thermal field originated from SRS in optical fiber, its intensity correlation function can be approximately written as

$$g^{(2)} = 1 + \frac{\Delta\tau_c}{\sqrt{\Delta\tau_c^2 + \Delta T_p^2}}, \tag{38}$$

while for the thermal field originated from broadband SFWM, $g^{(2)}$ is given by

$$g^{(2)} = 1 + \frac{\Delta\tau_c}{\sqrt{\Delta\tau_c^2 + \Delta T_p^2/2}}, \tag{39}$$

where $\Delta T_p$ is the pulse duration of pump pulses and $\Delta\tau_c$ is the coherence time of detected thermal field [10,20]. The difference between the expressions in Eqs. (38) and (39) comes from the different radiation mechanics. SRS can be viewed as a three-photon process, but SFWM is a four-photon process. According to the relation between mode number $M$ and intensity correlation function $g^{(2)}$ of a thermal field [see Eq. (16)], $M$ can be easily altered by passing a broadband thermal field through a bandwidth tunable filter to change its coherence time.

The basis of TMs [see $\phi_i(t)$ and $\varphi_k(t)$ in Eqs. (18) and (19)] for each kind of TS is determined by the specific nonlinear process in the DSF and its pulsed pump field [21,22]. For SRS, the mode structure is mainly determined by the pump pulse duration, while, for SFWM, the mode structure is determined by both the phase matching condition and pump spectrum [23]. $E_1$ and $E_2$ with mode number greater than 1 and with identical temporal mode structure can be obtained only when the excitation conditions of $TS_1$ and $TS_2$ are exactly the same. When the parameters related to exciting nonlinear process are

changed, the basis of TMs will be accordingly altered. The two pumps of nonlinear media $DSF_1$ and $DSF_2$, $P_1$ and $P_2$, are polarized and are achieved by dividing the output of a mode locked fiber laser into two with a 50:50 beam splitter ($BS_1$). The repetition rate of the laser is about 36.88 MHz. The central wavelengths of the two Gaussian shaped pumps $P_1$ and $P_2$ are the same, but their bandwidth is respectively determined by the filter $F_1$ and $F_2$. The pulse duration of $P_{1,2}$ can be adjusted to be $\sim$5 or $\sim$10 ps, which is achieved by setting the bandwidth of $F_{1,2}$ to 1 or 0.4 nm. The power of $P_1$ ($P_2$) is adjustable by using the combination of fiber polarization controller $FPC_1$ ($FPC_2$) and fiber polarization beam splitter $FPBS_1$ ($FPBS_2$).

In order to suppress the residual pump and conveniently change the mode number of two thermal fields, we propagate the output of $TS_{1,2}$ through a tunable filter $TF_{1,2}$ to adjust the coherence time $\Delta\tau_c$ of $E_{1,2}$ by varying its bandwidth. The central wavelength of $TF_{1,2}$ is the same as that of $E_{1,2}$ and can be tuned within the range of 1530–1570 nm. The pulse duration of $E_{1,2}$, determined by the pump pulse width and bandwidth of $TF_{1,2}$, is within tens of picosecond. It is well known that, when $E_{1,2}$ can be viewed as in single mode and the coherence time of $E_{1,2}$ (inversely proportional to the bandwidth of $TF_{1,2}$) is much longer than the pulse duration of $TS_{1,2}$, the spectrum of $TF_{1,2}$ defines the mode property of $E_{1,2}$ [9]. However, in this paper, we are mainly interested in $E_1$ and $E_2$ with mode number $M_{1,2} > 1$. So the tunable filter $TF_{1,2}$ will has no effect on TMs basis of $E_{1,2}$, but changes the weight of each eigenmode, which corresponds to the coefficients $\alpha_i$ and $\beta_k$ of the specified TMs $\phi_i(t)$ and $\varphi_k(t)$ [see Eq. (20)].

Mixing two independent thermal fields at $BS_2$, we then obtain the interference field, $\vec{E}_m(t) = \frac{1}{\sqrt{2}}[\vec{E}_1(t) + \vec{E}_2(t + \tau)]$. The relative delay $\tau$ between $E_1$ and $E_2$ is introduced by passing the field $E_2$ through a delay line (DL) placed in front of $BS_2$. The interference effect of $E(t)$ is characterized by measuring its intensity correlation function with an HBT interferometer, consisting of a 50:50 BS ($BS_3$) and two single photon detectors, $SPD_1$ and $SPD_2$. The intensity correlation function is measured when the path lengths from $BS_3$ to $SPD_1$ and $SPD_2$, respectively, are equal. In order to conveniently

study the factors influencing the mode property of interference field, we change the mode number of $E_{1,2}$ by varying the FWHM of $TF_{1,2}$ in the range of 0.3 and 2.5 nm and adjust the relative intensity coefficient $\mathcal{R}$ [see Eq. (30)] by using the variable optical attenuators $VOA_1$ and $VOA_2$ to change the intensity of fields $E_1$ and $E_2$. Note that another function provided by the two VOAs is to ensure the intensity of an optical field incident on an SPD is far from its saturation limit.

The two SPDs (InGaAs-based) are operated in a gated Geiger mode. The 2.5 ns gate pulses coincide with the arrival of photons at SPDs. The response time of SPDs is about 1 ns, which is about 100 times longer than the pulse duration of the detected thermal fields. The electrical signals produced by the SPDs in response to the incoming photons are reshaped and acquired by a computer-controlled analog-to-digital (A/D) board. So the individual count rate of two SPDs, $N_1$ and $N_2$, and twofold coincidences acquired from different time bins can be determined because the A/D card records all counting events. The excess correlation of the thermal field is measured by the coincidence rate originated from the same time bin, $N_c$, and the normalized intensity correlation function of the interference field is then obtained from the relation $g_m^{(2)} = N_c/(N_1 N_2)$, where $N_1$ and $N_2$ are proportional to the intensity of detected fields. When the mode number of individual thermal field $M_{1,2}$ needs to be characterized, we directly sent $E_1$ or $E_2$ into the HBT interferometer to measure its intensity correlation function $g_{1,2}^{(2)}$. The mode number $M_{1,2}$ is then deduced through the relation $g_{1,2}^{(2)} = 1 + 1/M_{1,2}$.

### A. Interference field formed by mixing two thermal sources with identical mode structure

We first verify the upper bound and lower limit of the two-photon interference effect by using two TSs with the same mode profiles, which means the mode bases of $E_1$ and $E_2$ are perfectly overlapped. In this case, $\phi_i(t)$ and $\varphi_k(t)$ in Eqs. (18) and (19) are identical, i.e., $\phi_i(t) = \varphi_i(t)$. To achieve this, the thermal sources, $TS_1$ and $TS_2$, are the same in every detail. The Raman scattering process respectively occurring in two DSFs are identical to ensure exact similarity. In the experiments presented in this subsection, the two DSFs are identical. The length and zero dispersion wavelengths of each DSF are 300 m and 1552 nm. The central wavelengths of both $P_1$ and $P_2$ are selected to be 1541 nm, at which the phase matching condition of SFWM is not satisfied and only SRS occurs in DSF. Moreover, the FWHM and average power for both $P_1$ and $P_2$ are 1 nm and 1 mW, respectively.

In the experiment of verifying the upper bound of two-photon interference in the interference field, the central wavelengths of both $E_1$ and $E_2$ are 1564 nm, and relative delay is set to $\tau = 0$ by carefully adjusting the DL. Moreover, the polarizations for $E_1$ and $E_2$ at $BS_2$ are adjusted to be the same. Hence the conditions $\cos\theta = 1$ and $K_{ik} = \delta_{i,k}$ [in Eq. (25)] are satisfied. We conduct the measurement of $g_m^{(2)}$ for the interference field $E(t)$ when the bandwidth of $E_1$ is fixed at 0.75 nm but the bandwidth of $E_2$ is 0.75 and 2.25 nm, respectively. In the two cases, the mode numbers of $E_1$ and $E_2$ are (i) $M_1 = M_2 = 1.25$ and (ii) $M_1 = 1.25$, $M_2 = 2.5$. The data of $g_m^{(2)}$ for cases (i) and (ii) with $\mathcal{R} = 0.75, 0.5, 0.25$
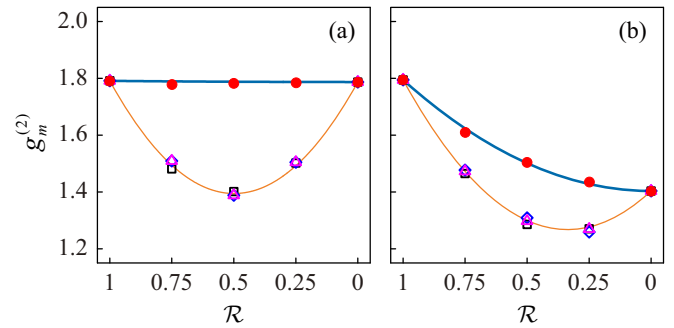


FIG. 4. Intensity correlation function of the interference field $g_m^{(2)}$ for two thermal fields $E_1$ and $E_2$ with different relative intensity coefficient $\mathcal{R}$. The results in (a) and (b) are obtained by fixing the mode number of $E_1$ at $M_1 = 1.25$ but setting the mode number of $E_2$ to $M_2 = 1.25$ and $M_2 = 2.5$, respectively. The error bars of data are within the size of data points. The solid circles are obtained for $E_1$ and $E_2$ with the mode profiles satisfying the upper bound conditions, $\cos\theta = 1$ and $K_{ik} = \delta_{ik}$, while others (squares, diamonds, and triangles) are obtained when the mode profiles of $E_1$ and $E_2$ satisfy the lower limit conditions, $\cos\theta = 0$ or $K_{ik} = 0$. The thick and thin curves are the results calculated by substituting mode numbers of $E_1$ and $E_2$ into upper bound and lower limit of $g_m^{(2)}$ in Eqs. (29) and (32), respectively.

is represented by the solid circles in Figs. 4(a) and 4(b), respectively. As a comparison, we calculate $g_m^{(2)}$ as a function of $\mathcal{R}$ by substituting the experimental parameters into Eq. (29), as shown by the thick solid curves in Figs. 4(a) and 4(b), respectively. The results indicate that the theoretical prediction for the upper bound fits the experimental data very well.

In the experiment of verifying the lower limit of two-photon interference in interference field, the experimental parameters are the same as those for verifying the upper bound, except the polarization states of $E_1$ and $E_2$ in front of the $BS_2$ are orthogonal ($\vec{e}_1 \perp \vec{e}_2$) or the delay between $E_1$ and $E_2$ at the $BS_2$ is adjusted by DL so that the approximation $\tau \to \infty$ is valid. Therefore, the condition of $\cos\theta = 0$ or $K_{ik} = 0$ in Eq. (25) is satisfied. We conduct the measurement of $g_m^{(2)}$ for the interference field under the condition of $\vec{e}_1 \perp \vec{e}_2$ or $\tau \to \infty$ when the relative strength of the two thermal fields is $\mathcal{R} = 0.75, 0.5, 0.25$. In the measurement, the results for the two kinds of mode number combinations for $E_1$ and $E_2$, the same as cases (i) and (ii) for verifying the upper bound, are shown in Fig. 4. The data obtained under the condition of orthogonal polarization ($\vec{e}_1 \perp \vec{e}_2$) and negligible overlap in time domain ($\tau \to \infty$), respectively, is represented by the hollow squares and diamonds in Figs. 4(a) and 4(b). As a comparison, we substitute the experimental parameters into Eq. (32) to calculate the corresponding $g_m^{(2)}$ by varying $\mathcal{R}$, as shown by the thin solid curves in Figs. 4(a) and 4(b), respectively. It is obvious that the theoretical prediction of the lower limit perfectly agrees with the experimental results. Additionally, we also achieve $K_{ik} = 0$ by adjusting the central wavelength of $E_1$ field from 1564 nm to 1566 nm using $TF_1$, which leads to the orthogonality of $E_1$ and $E_2$ as well. By keeping the other parameters the same as those for testing the upper bound, we measure $g_m^{(2)}$ for $\mathcal{R} = 0.75, 0.5, 0.25$. The data for the mode number the same as cases (i) and (ii) are shown as
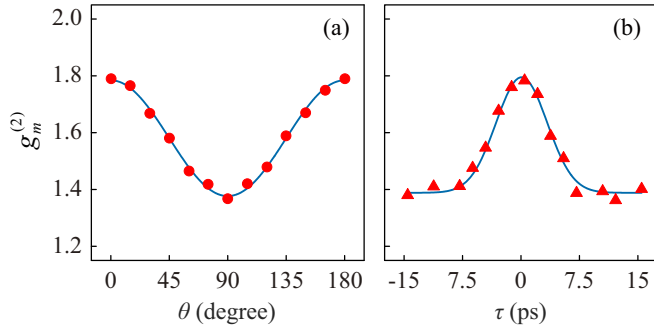
FIG. 5. Intensity correlation function of the interference field $g_m^{(2)}$ measured by (a) varying the angle of the polarization $\theta$ between linearly polarized $E_1$ and $E_2$ and by (b) varying the delay $\tau$ between $E_1$ and $E_2$. In the measurement, $M = M_1 = M_2 = 1.25$ ($g_m^{(2)} = g_1^{(2)} = g_2^{(2)} = 1.8$) and $\mathcal{R} = 0.5$. The error bars of data are within the size of data points. The solid curves in (a) and (b) are obtained by substituting experimental parameters in the formulas $g_m^{(2)} = 1 + \frac{1}{2M}(1 + \cos^2\theta)$ and $g_m^{(2)} = 1 + \frac{1}{2M}\{1 + \exp[-\tau^2\sigma^2(g^{(2)} - 1)^2/2]\}$, respectively.

the hollow triangles in Figs. 4(a) and 4(b), respectively, which overlap with the hollow squares and diamonds and well fit the theoretical curves for the lower limit.

We next study the influence of the mode mismatch effect on two-photon interference by changing $K_{ik}$ or $\cos\theta$ in Eq. (25) from zero to 1. We achieve this by adjusting the delay or polarization angle between the linearly polarized fields $E_1$ and $E_2$, and by keeping other experimental parameters the same as those for verifying the upper bound. In this experiment, the intensities for both $E_1$ and $E_2$ are the same, and the mode numbers for both $E_1$ and $E_2$ are fixed at 1.25. The solid circles in Fig. 5(a) present measured $g_m^{(2)}$ as a function of the angle $\theta$ between the polarization of $E_1$ and $E_2$ under the condition of $\tau = 0$. Moreover, we calculate $g_m^{(2)}$ by substituting the experimental parameters, $\mathcal{R} = 0.5$ and $M = M_1 = M_2 = 1.25$, into the formula $g_m^{(2)} = 1 + \frac{1}{2M}(1 + \cos^2\theta)$ [a simplified form of Eq. (25)], which agrees well with the experimental data. The triangles in Fig. 5(b) present the measured $g_m^{(2)}$ as a function of relative delay $\tau$ under the condition of $\vec{e}_1 \cdot \vec{e}_2 = 1$. Since the mode profiles of $E_1$ and $E_2$ are the same, the effect of delay can be calculated by using Eq. (13) in Ref. [10]. In this way, we have $g_m^{(2)} = 1 + \frac{1}{2M}\{1 + \exp[\frac{-\tau^2(g^{(2)}-1)^2}{2\tau_c^2}]\}$, where the coherence time of the thermal field is determined by spectral bandwidth $\sigma$ of thermal fields through the relation $\tau_c = \frac{1}{\sigma}$. Substituting the experimental parameters into the formula, we obtain the solid curve in Fig. 5(b), which is well fitted with the experimental results.

### B. Interference field formed by mixing two thermal sources with different mode structure

The results in Figs. 4 and 5 demonstrate that our theoretical analysis is correct for two independent thermal sources having the same temporal mode structures. In nature, thermal fields obtained from different kinds of sources usually have different mode structure. In this case, $0 < K_{ik} < 1$, even for $E_1$ and $E_2$ with zero delay ($\tau = 0$), perfect polarization states ($\vec{e}_1 \cdot \vec{e}_2 = 1$), and identical spectrum. In this subsection, we will perform
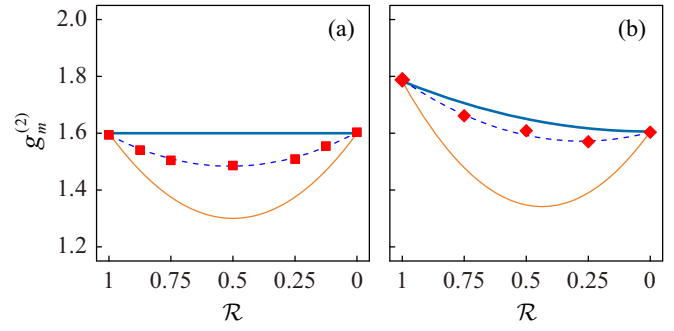


FIG. 6. Intensity correlation function $g_m^{(2)}$ of the interference field formed by mixing two thermal fields $E_1$ and $E_2$ varies with different relative intensity coefficient $\mathcal{R}$. The squares and diamonds are obtained for $E_1$ and $E_2$ with mode numbers of (a) $M_1 = M_2 = 1.67$ and (b) $M_1 = 1.25$, $M_2 = 1.67$, respectively. The error bars of data are within the size of data points. The dashed curves are fittings of Eq. (35) with $\mathcal{V} = 0.62$ for (a) and 0.82 for (b). The thick and thin curves are the theoretical predictions of upper bound and lower limit, calculated by substituting mode numbers of $E_1$ and $E_2$ into Eqs. (29) and (32), respectively. In the measurement, $E_1$ and $E_2$ are originated from two independent spontaneous Raman scattering processes with different basis of temporal modes; the conditions $0 < K_{i,k} < 1$ and $\cos\theta = 1$, $\tau = 0$ are satisfied.

experiments when the TMs bases of $E_1$ and $E_2$ are partially overlapped. To obtain the two thermal sources with different mode profiles, we proceed with two approaches.

The first approach still utilizes spontaneous Raman scattering as two independent thermal sources, but the pulse durations of two pumps are different. So the TMs bases of $TS_1$ and $TS_2$ are different. In this case, the experimental parameters are the same as those for verifying the upper bound of interference, but the pulse duration of the two pump fields, $P_1$ and $P_2$, are set to about 5 and 10 ps, respectively. Moreover, $E_1$ is obtained by passing the output of $DSF_1$ through $TF_1$ with FWHM of 0.75 nm or 1.3 nm, which correspond to the average mode number of $M_1 = 1.25$ or $M_1 = 1.67$ ($g_1^{(2)} = 1.8$ or $g_1^{(2)} = 1.6$). $E_2$ is obtained by passing the output of $DSF_2$ through $TF_2$ with FWHM of 0.5 nm, which corresponds to the average mode number $M_2 = 1.67$ ($g_2^{(2)} = 1.6$). For $E_1$ and $E_2$ with the two kinds of mode number combinations, we measure $g_m^{(2)}$ of the interference field $E(t)$ when the relative strength coefficient of $E_1$ and $E_2$ is $\mathcal{R} = 0.75, 0.5, 0.25$, as shown by the solid squares and diamonds in Figs. 6(a) and 6(b), respectively. We fit the data by using Eq. (35) (dashed curves) with a best-fitting value of $\mathcal{V} = 0.62$ for Fig. 5(a) and $\mathcal{V} = 0.82$ for Fig. 5(b). As a comparison, we also plot the upper bound (thick curves) and lower limit (thin curves) of $g_m^{(2)}$ as a function of $\mathcal{R}$ by substituting the experimental parameters into Eqs. (29) and (32), respectively. It is clear that the experimental data of $g_m^{(2)}$ is within the upper bound and lower limit of the interference field due to the partial mode overlap between the TMs basis of $E_1$ and $E_2$. The fitting parameter $\mathcal{V}$ is within the range of $0 < \mathcal{V} < 1$, which qualitatively agrees with the theoretical prediction in Eq. (35).

The second approach is to switch the thermal source $TS_1$ to SFWM in DSF and keep the other, $TS_2$, the same as before. In
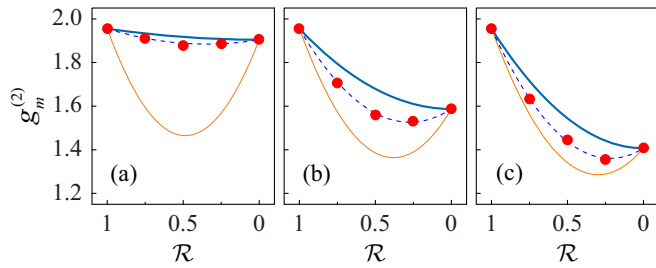
FIG. 7. Intensity correlation function of interference field $g_m^{(2)}$ versus the relative intensity coefficient $\mathcal{R}$ when the mode numbers of thermal field $E_1$ are fixed at $M_1 = 1.05$ but the mode number of thermal field $E_2$ is (a) $M_2 = 1.11$, (b) $M_2 = 1.67$, and (c) $M_2 = 2.5$, respectively. The error bars of data are within the size of data points. The dashed curves are obtained by fitting the data (solid circles) to Eq. (35) (dashed curves) with the best-fit value $\mathcal{V} = 0.93$ for (a), 0.62 for (b), and 0.48 for (c), respectively. The thick and thin curves, representing the upper bound and lower limit of the interference effect, are calculated by substituting mode numbers of $E_1$ and $E_2$ into Eqs. (29) and (32), respectively. In the measurement, $E_1$ and $E_2$ are originated from the nonlinear processes of spontaneous four wave mixing and spontaneous Raman scattering, respectively, and the conditions $0 < K_{ik} < 1$ and $\cos\theta = 1$, $\tau = 0$ are satisfied.

this case, TS$_1$ is replaced by using another DSF having zero dispersion wavelength at 1540 nm. With this replacement, the phase matching condition of SFWM in DSF$_1$ is satisfied. Moreover, we increase the pump power P$_1$ from 1 mW to 2 mW, so that the gain of four wave mixing is quite high and the intensity of Raman scattering (RS) in DSF$_1$ is negligible [22]. As a result, up to 98% photons in thermal field $E_1$ are originated from the individual Stokes field of SFWM, while the field $E_2$ from DSF$_2$ is still radiated by RS. So the mode profiles of TS$_1$ and TS$_2$ are quite different. Moreover, $E_1$ is obtained by passing the output of DSF$_1$ through TF$_1$ with FWHM of 0.3 nm, which corresponds to average mode number $M_1 = 1.05$ ($g_1^{(2)} = 1.95$), while $E_2$ is obtained by passing the output of DSF$_2$ through TF$_2$ with FWHM of 0.5, 1.5, and 2.5 nm, which correspond to the mode number of $M_2 = 1.11$, 1.67, and 2.5, respectively. For $E_1$ and $E_2$ with the three kinds of mode number combinations, we then measure $g_m^{(2)}$ of the interference field $E(t)$ when the relative strength coefficient of $E_1$ and $E_2$ is $\mathcal{R} = 0.75, 0.5, 0.25$, as shown by the solid circles in Figs. 7(a), 7(b), and 7(c), respectively. The data is fitted to Eq. (35) (dashed curves) with the best-fit value $\mathcal{V}$ of 0.93, 0.62, and 0.48, respectively. Additionally, according to the three kinds of mode number combinations of $M_1$ and $M_2$, we calculate the upper and lower bounds of $g_m^{(2)}$ as a function of $\mathcal{R}$ by using Eqs. (29) and (32), as shown by the thick and

thin solid curves in Figs. 7(a), 7(b), and 7(c), respectively. Similar to Fig. 6, the experimental results of $g_m^{(2)}$ in Fig. 7 are within the upper and lower bounds, which agree with the theoretical prediction in Eq. (35). Moreover, we notice that, in this experiment, $E_1$ field is very close to single mode, so its mode profile here can be approximated by the spectrum of TF$_1$ [9,10]. In this case, it is reasonable that the fitting parameter $\mathcal{V}$, reflecting the degree of mode mismatching between $E_1$ and $E_2$, decreases with the increase of $M_2$.

## IV. CONCLUSIONS AND DISCUSSION

We have developed a general theory for analyzing the intensity correlation function $g_m^{(2)}$ of the interference field formed by mixing two independent multi-temporal-mode thermal fields. We derive the analytical expression of $g_m^{(2)}$ for two thermal fields with their mode structures identical, orthogonal, and partially overlapped, respectively. Comparing with $g^{(2)}$ for one of the individual thermal fields with less average mode number, we find $g_m^{(2)}$ of the interference field always decreases, but the amount of drop depends on the relative overlap between the mode structures of the two thermal fields and their relative strength. Moreover, we perform experiments to verify the theory.

Although the analytical expression of $g_m^{(2)}$ is deduced under a rough assumption of Eq. (28), the experimentally measured $g_m^{(2)}$ well agrees with the theoretical predictions, no matter the modes of two multi-temporal-mode thermal fields involved in the interference are identical, orthogonal, or partially overlapped, as long as the temporal mode bases of two thermal sources are the same. On the other hand, when the temporal mode bases of two thermal sources are not identical but partially overlapped, the experimental results qualitatively agree with the prediction in Eq. (35). We believe this is because the assumptions in Eq. (28) used to deduce Eq. (35) from Eq. (25) deviate from the thermal sources used in experiment. In order to precisely predict the theoretical curve of $g_m^{(2)}$ in this case, instead of using the general theory in Sec. II, we need to resort to a theoretical model for describing the specific nonlinear process [21,22,24,25], from which the details of TMs for each thermal source can be obtained and the accurate simulation of $g_m^{(2)}$ can be fulfilled [23]. We believe our investigation is useful for analyzing the signals carried by the intensity correlation function of thermal fields, such as improving the SNR of ghost imaging and analyzing the mode property of multi-mode quantum field [3,12].

[1] R. Loudon, *The Quantum Theory of Light*, 3rd ed. (Oxford University Press, Oxford, 2000).

[2] R. H. Brown and R. Q. Twiss, Nature (London) **177**, 27 (1956).

[3] A. Valencia, G. Scarcelli, M. D'Angelo, and Y. H. Shih, Phys. Rev. Lett. **94**, 063601 (2005).

[4] P. Ryczkowski, M. Barbier, A. T. Friberg, J. M. Dudley, and G. Genty, Nat. Photon. **10**, 167 (2016).

[5] D. Fabrice, H. Kien Phan, D. Séverine, L. Eric, and M. Paul-Antoine, J. Opt. **19**, 024001 (2017).

[6] R. L. Pfleegor and L. Mandel, Phys. Rev. **159**, 1084 (1967).

[7] L. Mandel, Rev. Mod. Phys. **71**, S274 (1999).

[8] L. Mandel, Phys. Rev. A **28**, 929 (1983).

[9] Z. Y. Ou, J.-K. Rhee, and L. J. Wang, Phys. Rev. A **60**, 593 (1999).

[10] X. Ma, X. Li, L. Cui, X. Guo, and L. Yang, Phys. Rev. A **84**, 023829 (2011).

[11] L. Mandel and E. Wolf, *Optical Coherence and Quantum Optics* (Cambridge University Press, New York, 1995).

[12] B. Brecht, D. V. Reddy, C. Silberhorn, and M. G. Raymer, Phys. Rev. X **5**, 041017 (2015).

[13] B. Yurke and M. Potasek, Phys. Rev. A **36**, 3464 (1987).

[14] Z. Y. Ou, *Quantum Optics for Experimentalists* (World Scientific, Singapore, 2017).

[15] L. Yang, X. Ma, X. Guo, L. Cui, and X. Li, Phys. Rev. A **83**, 053843 (2011).

[16] M. Koashi, K. Kono, T. Hirano, and M. Matsuoka, Phys. Rev. Lett. **71**, 1164 (1993).

[17] L. Isserlis, Biometrika **12**, 134 (1918).

[18] X. Li, P. L. Voss, J. Chen, K. F. Lee, and P. Kumar, Opt. Express **13**, 2236 (2005).

[19] G. Agrawal, *Nonlinear Fiber Optics* (Elsevier Science, Amsterdam, 2012).

[20] P. R. Tapster and J. G. Rarity, J. Mod. Opt. **45**, 595 (1998).

[21] X. Li, X. Ma, Z. Y. Ou, L. Yang, L. Cui, and D. Yu, Opt. Express **16**, 32 (2008).

[22] N. Liu, Y. Liu, X. Guo, L. Yang, X. Li, and Z. Y. Ou, Opt. Express **24**, 1096 (2016).

[23] X. Ma, L. Cui, and X. Li, J. Opt. Soc. Am. B **32**, 946 (2015).

[24] K. Garay-Palmett, H. J. McGuinness, O. Cohen, J. S. Lundeen, R. Rangel-Rojo, A. B. U'Ren, M. G. Raymer, C. J. McKinstrie, S. Radic, and I. A. Walmsley, Opt. Express **15**, 14870 (2007).

[25] O. Cohen, J. S. Lundeen, B. J. Smith, G. Puentes, P. J. Mosley, and I. A. Walmsley, Phys. Rev. Lett. **102**, 123603 (2009).

*Correction:* The surname of the second author contained a spelling error and has been corrected.